On the universality of Keane & Adrian's valid detection probability in PIV

On the universality of Keane & Adrian's valid detection probability in PIV

Sven Scharnowski[1] , **Andrea Sciacchitano**[2] and **Christian J Kähler**[1]

1 Institute of Fluid Mechnics and Aerodynamics, Bundeswehr University Munich, Neubiberg, Germany
2 Department of Aerospace Engineering, Delft University of Technology, 2629HS Delft, The Netherlands

E-mail: sven.scharnowski@unibw.de

CrossMark

Abstract

For the reliable estimation of velocity vector fields by means of particle image velocimetry (PIV), the cross-correlation functions calculated from the signal within each interrogation window must feature a distinct peak that represents the average shift of the particle image ensemble. A high valid detection probability (VDP) of the correct correlation peak is necessary in order to compute valid but also accurate velocity fields. According to Keane and Adrian it is believed that the so-called effective number of particle images $N_I F_I F_O$ must be around 6 to obtain 95% valid detection probability (Keane and Adrian 1992 *Appl. Sci. Res.* **49** 191–215). To prove the findings of Keane and Adrian, this work examines the sensitivity of the VDP on image parameters, flow parameters as well as on evaluation parameters in more detail. The most important result is that the effective number of particle images $N_I F_I F_O$ is not suited to predict the VDP in the case of moderate or strong out-of-plane motion. This can be explained by the fact that the VDP depends not only on the number of particle images correctly paired, but also on the number of particle images remaining without partner, which yield spurious correlation peaks. This point remained unnoticed in the work of Keane and Adrian. The findings of this investigation help to better understand the occurrence of false vectors and enable the PIV user to improve the measurement setup as well as the PIV evaluation in order to minimize spurious vectors.

Keywords: PIV, cross-correlation function, uncertainty quantification

(Some figures may appear in colour only in the online journal)

1. Introduction

In particle image velocimetry (PIV) the velocity of a group of particles is estimated from the cross-correlation function of two interrogation windows containing the corresponding particle images at two consecutive time instants [2–5]. Under ideal conditions, the sub-pixel location of the highest correlation value corresponds to the displacement of the particle image ensemble within the interrogation window. However, this only holds for the case where the flow within the interrogation window is uniform as well as homogeneously seeded

and a sufficient large number of particle images from two corresponding images can be paired. Furthermore, the particle size must be identical and the illumination must be uniform to ensure that the size and the brightness of the particle images is similar. Keane and Adrian [1] showed that the formation of a well detectable correlation peak is almost certain if the number of particle images within the interrogation window is $N_I \geqslant 6$. For $N_I < 6$, the likelihood that a random peak in the correlation function, that does not correspond to the correct particle image displacement, is higher than the one corresponding to the displacement, increases strongly. The valid detection probability VDP is the probability that the highest correlation peak corresponds to the true mean displacement of the particle image ensemble [1, 6].

For realistic PIV images, the loss-of-correlation due to in-plane motion F_I, out-of-plane motion F_O, displacement

gradients F_Δ or image noise F_σ lead to a decreased probability for the detection of valid displacement vectors [4, 5, 7–12]. Additionally, the reliable detection of the displacement peak's location becomes difficult under these conditions. The shape of the correlation peak [13, 14] as well as the ratio between the heights of the displacement peak and the second highest peak [15, 16] can be used to estimate the shift vector uncertainty.

Keane and Adrian concluded that for single exposed PIV double images the loss of correlation can be compensated by increasing the number of particle images N_I such that:

$$N_I F_I F_O \geqslant 6. \tag{1}$$

The product $N_I F_I F_O$ is the so-called effective number of particle images according to Keane and Adrian [1].

New investigations show that relation (1) is not sufficient if the number of unpaired particle images is of the same order as the number of paired ones or even higher. This is often the case for realistic experiments where the time between the two illuminations is optimized for low uncertainty and high spatial resolution. To achieve a low uncertainty and high spatial resolution at the same time, the particle image displacement must be large compared to the random error of the evaluation method [17]. Additionally, the light sheet must be thin and the interrogation windows must be small to achieve good out-of-plane and in-plane resolution, respectively. However, a large displacement in a thin light sheet also increases the probability of loss-of-pairs due to in-plane and out-of-plane motion and thus decreases F_I and F_O. Figure 1 illustrates how the valid detection probability changes with respect to the effective number of particle images over a wide range of particle image densities and interrogation window sizes. The number of particle images N_I within a squared interrogation window with an edge length of D_I is related to the particle image density as follows.

$$N_I = N_{ppp} \cdot D_I^2. \tag{2}$$

Where N_{ppp} is the average number of particle images per pixel.

The valid detection probability was evaluated from O(1000) correlation functions computed from synthetic PIV images for each data point in the figure. It can be concluded from figure 1 that the product $N_I F_I F_O$ is not useful in general to determine the effective number of particle images. Especially if N_I is relatively large and F_O is relatively small the unpaired particle images affect the correlation function significantly. For example $N_I = 10$ and $F_O = 1$ (red squares in figure 1) does not result in the same valid detection probability as $N_I = 100$ and $F_O = 0.1$ (black squares in figure 1). Although the product $N_I F_I F_O$ is constant, the valid detection probability decreases from 100% to about 7%. Thus, the rule of thumb that predicts a valid detection probability of $> 95\%$ for $N_I F_I F_O \geqslant 6$, does not apply if the parameters are varied over a large domain. In order to understand why the so-called effective number of particle images is not sufficient to predict the valid detection probability, the correlation functions of synthetic PIV images were analyzed systematically. The aim of this work is to identify the parameters that influence the VDP and to identify their suitable range for reliable PIV measurements.

The following section discusses the height distribution of the displacement peak as well as the secondary correlation peak and their relation to the valid detection probability. In section 3 the effect of several parameters on the valid detection probability is discussed in detail. Section 4 analyzes the possibility to optimize the interrogation window size depending on the flow and image parameters and conclusions are drawn in section 5.

2. Correlation peak height distribution and valid detection probability

Figure 2 shows an example of a synthetic PIV image pair with a relative out-of-plane shift of $\Delta z/\Delta z_0 = 0.3$ corresponding to $F_O = 0.7$, with Δz_0 being the thickness of a top-hat light sheet. The in-plane-shift was set to zero, to simulate the second or any later pass of a multi-pass evaluation. On average 12.8 particle images are found in each interrogation window of size $D_I = 16$ pixel for a particle image density (number of particle images per pixel) of $N_{ppp} = 0.05$. However, as can be seen from the figure, the true number of particle images within each window varies significantly. For randomly chosen locations, the probability of finding exactly N_I particle image centers within a D_I^2 window is given by the binomial distribution:

$$pdf(N_I, D_I, N_{ppp}) = \binom{D_I^2}{N_I} \cdot N_{ppp}^{N_I} \cdot (1 - N_{ppp})^{D_I^2 - N_I} \tag{3}$$

where D_I is the interrogation window size expressed in pixel. The distribution in figure 3 clearly shows a strong variation of N_I in agreement with the randomly distributed particle images in figure 2. The probability of finding 12 particle images within a window is about 11.4% but extreme values such as 6 and 20 particle images have still a significant probability of about 1.5%.

On the right side of figure 2 the normalized cross-correlation functions of the interrogation windows of the two PIV images are shown qualitatively. The true displacement peak and the secondary peak are marked by circles and squares, respectively. Blue color of the circles and squares indicates the highest peak while the second highest peak is colored in red. It can be seen from the figure that the secondary peak is sometimes higher than the displacement peak (refer to second and third row from top in the most right column). This is mainly caused by a low number of particle images within the interrogation window in combination with loss-of-correlation due to out-of-plane loss-of-pairs. In the case of valid measurements, the displacement peak is higher than the secondary peak, and a valid vector is detected. Instead, when the secondary peak is larger than the displacement peak, an erroneous displacement vector (outlier or spurious vector) is computed. In the latter case, the spurious vectors can be identified and removed based on their difference to neighboring vectors if the spurious vectors appear separately and do not form clusters [18]. To avoid clusters of erroneous displacement vector, it is recommended to use an interrogation window size that results in a valid detection probability of 95% [5]. Additionally, the search radius for finding the displacement peak can be decreased
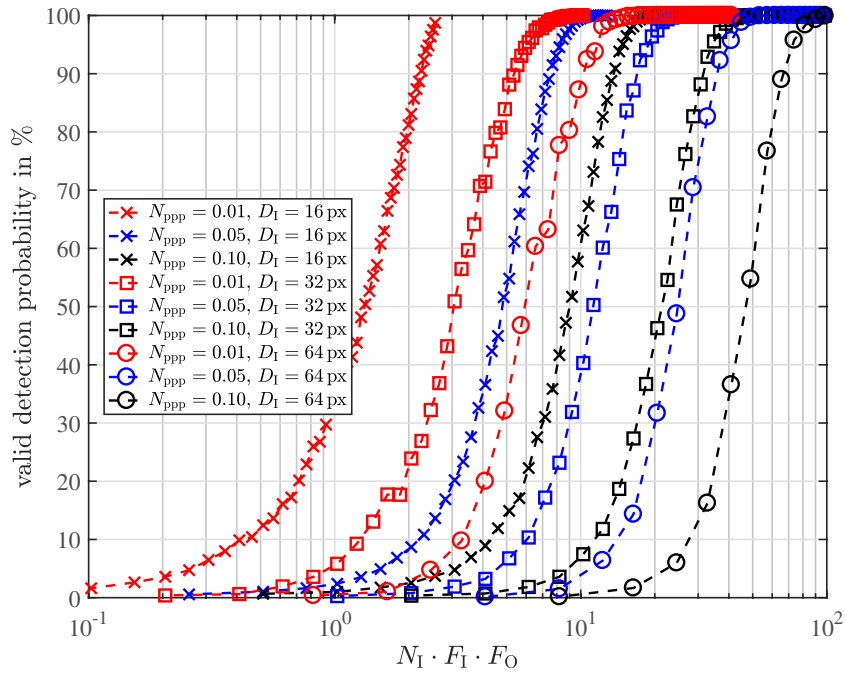
Figure 1. Valid vector detection probability as a function of the effective number of particle images $N_I F_I F_O$ for synthetic PIV images with zero in-plane motion ($F_I = 1$) and varying out-of-plane motion ($F_O = 0 \ldots 1$) for different particle image densities N_{ppp} and interrogation window sizes D_I.
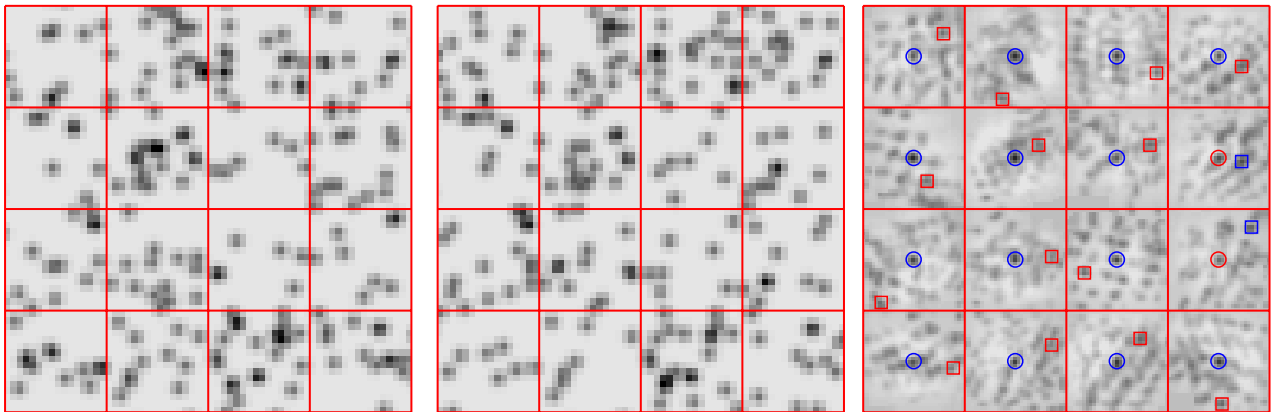
Figure 2. Example PIV double image with a particle image diameter of $D = 3$ pixel, a particle image density of $N_{ppp} = 0.05$ and an out-of-plane motion of $\Delta z / \Delta z_0 = 0.3$ (left and middle). Right: corresponding normalized correlation functions computed from an interrogation window size of $D_I = 16$ pixel. The true displacement peak and the secondary peak are marked by circles and squares, respectively. Blue and red color of the circles and squares indicates the highest and second highest peak, respectively.

in order to decrease the number of outliers. This approach requires prior knowledge about the flow field and is therefore only suited for the second and following passes of multi-pass PIV evaluation including image shifting [19] or image deformation [20]. Masullo and Theunissen [21] showed recently that image deformation can be improved by the analysis of multiple strong correlation peaks, which appear in the case of strong gradients within the interrogation window.

Figure 4 illustrates the distribution of the height of the displacement peak and the secondary correlation peak for the case with significant out-of-plane shift $\Delta z / \Delta z_0 = 0.3$. The correlation peak heights were analyzed by means of synthetic PIV images with zero in-plane motion as shown in figure 2. The particle image diameter, the particle image density and the interrogation window size were set to $D = 3$ pixel,

$N_{ppp} = 0.05$ and $D_I = 16$ pixel, respectively. The search radius for the secondary correlation peak was limited to half the interrogation window size ($\pm D_I / 2$). Figure 4 shows that for the majority of correlation functions the displacement peak is higher than the secondary peak within the search radius. However, for some cases the displacement peak becomes smaller than the secondary one, leading to an erroneous displacement vector. This is in agreement with the correlation functions presented in figure 2.

The actual value of the valid detection probability VDP depends on the probability density function of the displacement peak pdf_1 and of the secondary peak pdf_2 as follows:

$$\text{VDP} = \int_0^1 pdf_2(c_2) \cdot \int_{c_2}^1 pdf_1(c_1) \, dc_1 \, dc_2. \tag{4}$$
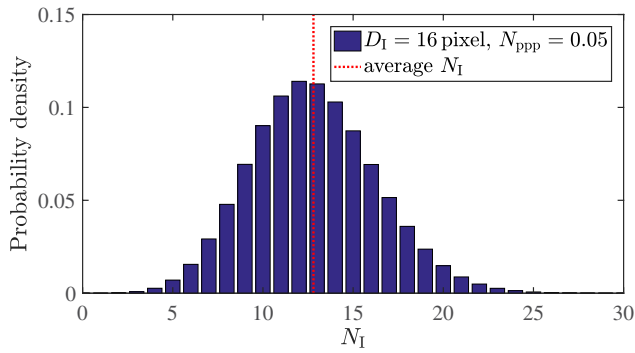
Figure 3. Probability density distribution of the number of particle images within a 16×16 pixel interrogation window for an average particle image density of $N_{\mathrm{ppp}} = 0.05$.
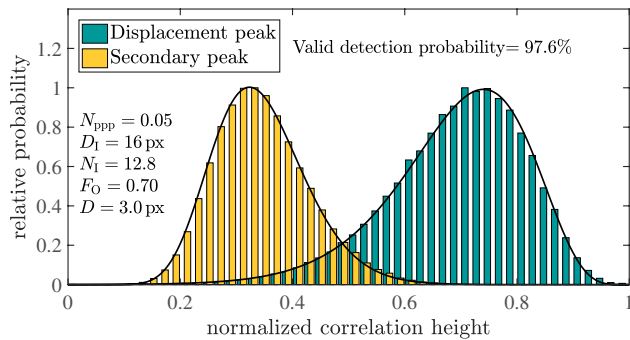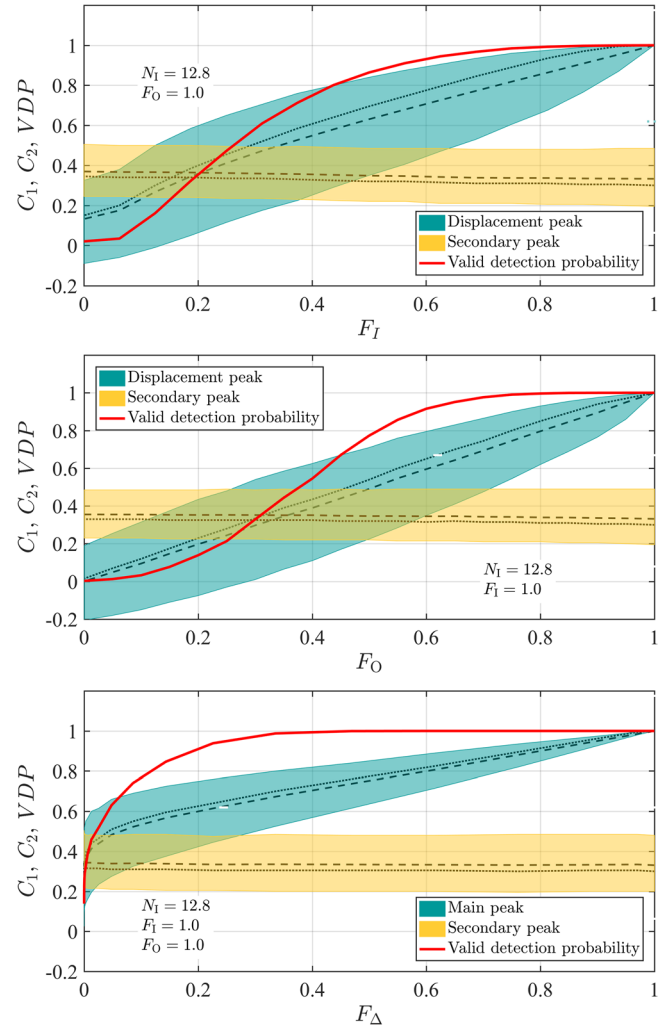

Figure 4. Probability density distribution of the normalized correlation height for the displacement peak and the secondary peak for $D = 3$ pixel, $D_{\mathrm{I}} = 16$ pixel, $N_{\mathrm{ppp}} = 0.05$ and $F_{\mathrm{O}} = 0.7$.

Where c_1 is the normalized height of the displacement peak and c_2 the normalized height of the secondary peak. It is important to note that equation (4) is only valid for normalized correlation functions. For non-normalized correlation functions the distributions of the height of the displacement peak and that of the secondary peak are not independent and cannot be separated as shown in the equation. For the case shown in figure 4 a valid detection probability of 97.6% is computed from the height distributions. Thus, for 2.4% of the cases the secondary peak becomes larger than the displacement peak.

3. Effect of image, flow and evaluation parameters on correlation statistic
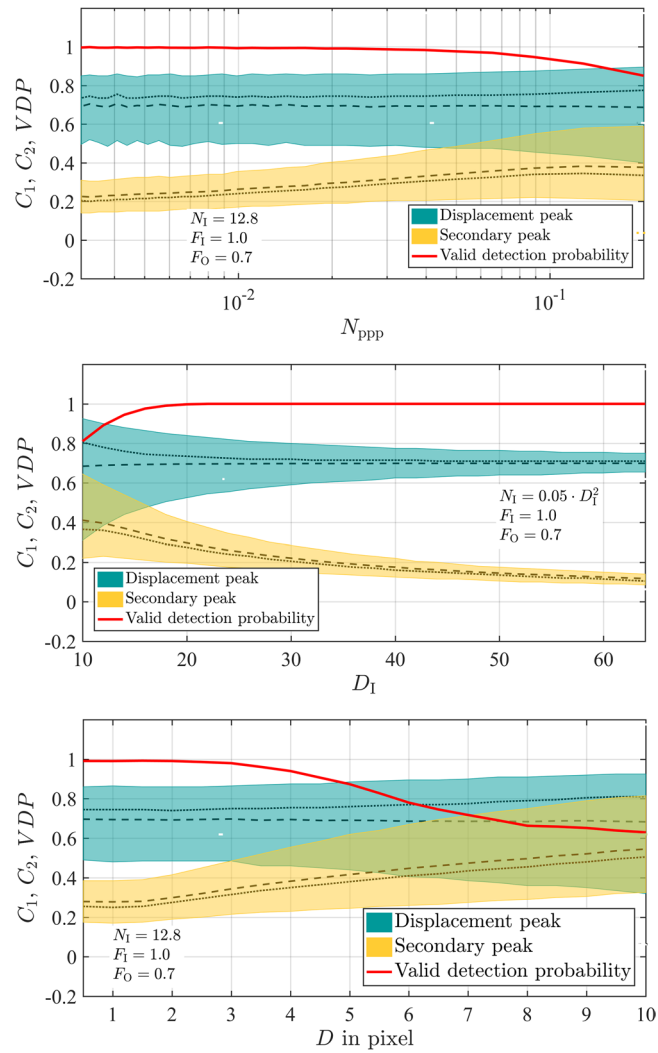
In order to understand the effect of different image parameters, flow parameters and evaluation parameters on the valid detection probability, synthetic PIV images with varying properties were generated and analyzed. Figure 5 shows the distributions of the height of the displacement peak and the secondary correlation peak for a variation of the in-plane-motion (top), the out-of-plane motion (middle) and the in-plane gradients (bottom). It is important to note that the three parameters in figure 5, F_{I}, F_{O}, and F_{Δ}, do not alter the probability of the secondary peak. This is due to the fact that the locations of the unpaired particle images are random and therefore not influenced by these parameters. However, the width of the displacement peak height distribution increases with decreasing F_{I}, F_{O}, and F_{Δ}, indicating that a broader

Figure 5. Effect of F_{I} (top), F_{O} (middle) and F_{Δ} (bottom) on the height distribution of the displacement peak and the secondary peak of the normalized cross-correlation function. The dotted lines and the dashed lines indicate the highest probability and the mean height, respectively. The shaded areas represent the 90% coverage of the *pdf* and the red solid line is the valid detection probability VDP given by equation (4).
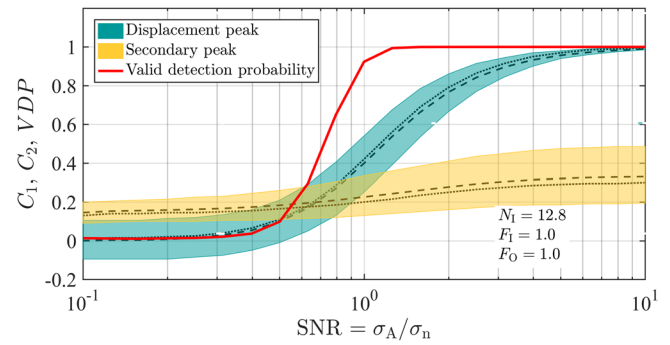
range of displacement peak heights becomes possible. If the displacement peak is always higher than the secondary peak the valid detection probability is unity. This is only the case if both peak height distributions are well separated, as shown for $F_{\mathrm{I}} > 0.65$, $F_{\mathrm{O}} > 0.7$, $F_{\Delta} > 0.3$.

In contrast to figure 5, the parameters analyzed in figure 6, N_{ppp}, D_{I}, and D, clearly influence the distribution of the secondary peak. The figure shows in the top row the effect of different particle image densities N_{ppp} on the correlation height distribution. The interrogation window size D_{I} was adjusted to keep the number of particle images constant at $N_{\mathrm{I}} = 12.8$. The displacement correlation peak is not affected for $N_{\mathrm{ppp}} < 0.1$ because it is still composed of the same number of particle images. For $N_{\mathrm{ppp}} > 0.1$ the particle images start to overlap massively leading to a slightly increasing width of pdf_1. The secondary peak however, depends on N_{ppp} over the full range: the width and the mean value of the distribution increase with increasing particle image density.

Figure 7. Effect of signal-to-noise ratio SNR on the height distribution of the displacement peak and the secondary peak of the normalized cross-correlation function. The dotted line and the dashed line indicate the highest probability and the mean height, respectively. The shaded areas represent the 90% coverage of the *pdf* and the red solid line is the valid detection probability VDP given by equation (4).

Figure 6. Effect of particle image density N_{ppp} (top), interrogation window size D_{I} (middle) and particle image diameter D (bottom) on the height distribution of the displacement peak and the secondary peak of the normalized cross-correlation function. The dotted lines and the dashed lines indicate the highest probability and the mean height, respectively. The shaded areas represent the 90% coverage of the *pdf* and the red solid line is the valid detection probability VDP given by equation (4).

Additionally, the interrogation window size D_{I} also affects the distribution of the secondary peak height pdf_2. Figure 6 illustrates in the middle row how the statistics of displacement peak and the secondary peak change with respect to the interrogation window size. The particle image density was kept constant at $N_{\mathrm{ppp}} = 0.05$. While the mean height of the displacement peak is rather constant, its width and the height with the highest probability (dotted line) increase with decreasing window size. The height and width of the secondary peak distribution is much more affected by D_{I}. With increasing interrogation window size more and more particle images contribute to the correlation function. This decreases the height of the secondary peak as well as the *pdf*'s width. As a result, the valid detection probability increases for larger interrogation window sizes, as expected. The best spatial resolution combined with reliable vector detection is reached as

soon as both *pdf* are separated, which is around $D_{\mathrm{I}} \approx 16$ pixel for the specific cases tested here.

The effect of the particle image size is illustrated in the bottom row of figure 6. It can be seen that larger particle images result in an increased height and a broader height distribution of the secondary correlation peak. As for the other parameters in the figure, the mean height of the displacement peak is rather unaffected. Consequently, the best valid detection probability is achieved for small particle images. However, in order to avoid bias errors due to peak locking, it is recommendet to select a particle image diameter between 2 and 3 pixel [22–24].

Image noise reduces the normalized correlation height of the displacement peak and the secondary peak, as shown in figure 7. In the region that is relevant for most experiments $\sigma_{\mathrm{A}}/\sigma_{\mathrm{n}} > 1$, the height of the displacement peak decreases much faster than the secondary one. Here σ_{A} is the intensity standard deviation of the noise-free image and σ_{n} is the image noise level [9].

In summary it can be stated that the *pdf* of the displacement peak and the secondary correlation peak is quite sensitive on flow parameters, image parameters and evaluation parameters. As a result, the estimation of the valid detection probability becomes rather complex and cannot be based solely on the parameter $N_{\mathrm{I}}F_{\mathrm{I}}F_{\mathrm{O}}$.

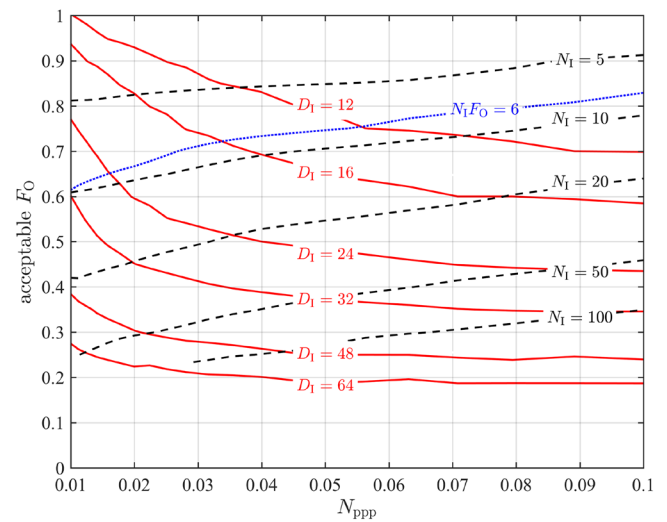## 4. Optimized interrogation window size

The strongest advantage of PIV over classical point-wise measurement techniques is its ability to provide flow fields from which the organization of flow structures of various length scales and intensity can be detected. In order to maximize the flow information acquired with PIV measurements, it is important to capture a large field of view and to resolve small details at the same time [25–27]. To achieve this, camera sensors with a large number of pixel or multiple camera approaches [28] can be combined with sophisticated image evaluation techniques that iteratively decrease the interrogation window size [20, 29].
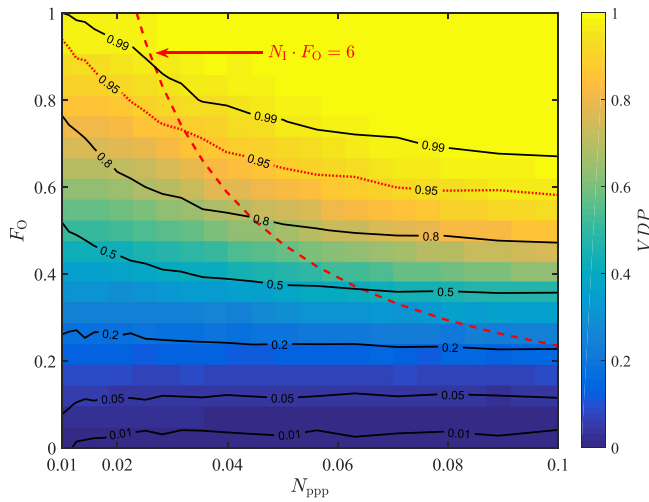
Figure 8. Valid detection probability VDP as a function of the particle image density N_{ppp} and the loss-of-correlation due to out-of-plane motion F_O for an interrogation window size of $D_I = 16$ pixel.

The optimum interrogation window size depends on several factors: for the first evaluation step, the in-plane motion as well as the in-plane gradients strongly affect the VDP. To account for this the shift of the particle image ensemble should not exceed one quarter of the interrogation window size [6]. However, this is only a constraint for the first iteration. For the following iterations the in-plane motion is compensated by window shifting and image deformation techniques so that the interrogation windows can be reduced in size from iteration to iteration. The smallest suited window size for a reliable detection of the mean shift of the particle image ensemble within the interrogation window is reached if only $N_I \approx 6$ particle images are found in each window on average [1]. Thus, the constraint of the particle image density limits the spatial resolution of PIV. If an out-of-plane motion is present the number of particle images within an interrogation window must be larger than 6, as illustrated in figure 1, to keep the valid detection probability on the same level. Additionally, for strong out-of-plane motions it is not sufficient to keep the product $N_I F_O \approx 6$, because the VDP also depends on the secondary correlation peak, which is formed from all particle images (see figure 4 and equation (4)). Furthermore, as shown in figure 6 in the top and middle row, the particle image density N_{ppp} and the number of particle images N_I influence the secondary correlation peak and thus the VDP.

The three parameters F_O, N_{ppp} and N_I are the driving parameters for determining the VDP. Figure 8 shows an example of the valid detection probability VDP as a function of F_O and N_{ppp} for an interrogation window of 16×16 pixel. It is clear from the figure, that a high valid detection probability (e.g. 95%) requires an increasing particle image density for smaller values of F_O in order to keep the spatial resolution constant. In other words: depending on the out-of-plane motion and the particle image density, the interrogation window size must be selected to ensure a sufficiently high VDP. In contrast to the findings of Keane and Adrian [1], the condition $N_I F_O > 6$ (dashed line in figure 8) is not sufficient to achieve VDP = 0.95.

Figure 9. Iso-lines with VDP = 0.95 showing the level of acceptable F_O with respect to the particle image density N_{ppp} for different interrogation window sizes (red solid lines). The dashed black lines indicate the required number of particle images within the interrogation window.

Figure 9 illustrates iso-contours with VDP = 0.95 for different interrogation windows between 12×12 and 64×64 pixel. The solid red lines in the figure show the acceptable value of F_O that results in VDP = 0.95 for each window size as a function of N_{ppp}. For smaller window sizes the VDP decreases and for larger ones the VDP increases. The dashed lines in figure 9 indicate the average number of particle images per interrogation window. The figure clearly shows that the condition $N_I F_O > 6$, as proposed by Keane and Adrian (1992), is not sufficient to achieve a high valid detection probability: for $N_I = 20$ and $N_{ppp} = 0.03$ the loss-of-correlation due to out-of-plane motion of $F_O \approx 0.5$ results in VDP = 0.95 although $N_I F_O \approx 10$, for example. The required effective number of particle images becomes even larger for cases with stronger out-of-plane motion and higher particle image density: for $N_I = 100$ and $N_{ppp} = 0.1$ the loss-of-correlation due to out-of-plane motion of $F_O \approx 0.35$ results in VDP = 0.95 although $N_I F_O \approx 35$. Furthermore, for $N_I F_O = 6$ (blue dotted line in figure 9) the loss-of-correlation due to out-of-plane motion must be $F_O > 0.6$ for the tested particle image density in order to achieve VDP > 0.95.

Figure 9 can be used in two ways. Knowing the seeding concentration (i.e. N_{ppp}) and selecting the interrogation window size D_I, one could determine the minimum value of F_O that still allows 95% valid detection probability. Such information can be used to increase the laser pulse separation to minimize the measurement uncertainty. Alternatively, for a given N_{ppp} and out-of-plane displacement (i.e. F_O), one could determine the minimum interrogation window size D_I that still allows VDP $\geqslant$ 95%, thus maximizing the spatial resolution.

5. Summary and conclusions

The analysis illustrates that the effective number of particle images $N_I F_I F_O$ is not sufficient to predict the valid detection probability of a PIV vector fields as proposed by Keane

and Adrian [1]. This is because not only the number of particle images that can be paired must be considered but also the number of those that cannot be paired is important. The former determine the height of the displacement peak and the latter contribute to the secondary correlation peak. Only if the number of paired particle images is large enough compared to the unpaired ones the correct correlation peak is the highest one.

Consequently, any image parameter, flow parameter or evaluation parameter that influences the height of the displacement peak or the secondary peak in the correlation function, also affects the valid detection probability. This was demonstrated in section 3. In order to achieve a high valid detection probability, the *pdf* of the displacement peak and the *pdf* of the secondary peak must be separated. This ensures that the displacement peak is always the highest peak in the correlation function. If the valid detection probability needs to be improved because the results are not satisfactory, the following points can be considered:

- Increasing the interrogation window size
- Reducing the time between the laser pulses
- Increasing the particle density
- Thickening the laser light sheet
- Reducing the particle image size
- Reducing the image noise level

It is important to note that modifying these parameters also changes the spatial resolution and/or the measurement uncertainty. An optimization regarding the spatial resolution and/or the uncertainty is recommended to be performed during data acquisition (time separation between double images, optical magnification, aperture, light sheet width and energy, particle concentration, ...) as well as during data evaluation (interrogation window size, image deformation approach, vector postprocessing, ...). The best spatial resolution is achieved once the *pdf* of the displacement peak and the *pdf* of the secondary peak are just separated. In this case, some outliers will appear and must be identified and rejected or replaced. The condition with best spatial resolution, corresponding to a VDP = 95%, is shown for a broad range of the most important parameters (N_I, F_O, N_{ppp}, D_I) in figure 9.

Acknowledgment

ORCID iDs

Sven Scharnowski ![ORCID] https://orcid.org/0000-0002-6452-2954
Andrea Sciacchitano ![ORCID] https://orcid.org/0000-0003-4627-3787

References

[1] Keane R D and Adrian R J 1992 Theory of cross-correlation analysis of PIV images *Appl. Sci. Res.* **49** 191–215
[2] Adrian R J 1984 Scattering particle characteristics and their effect on pulsed laser measurements of fluid flow: speckle velocimetry versus particle image velocimetry *Appl. Opt.* **23** 1690–1
[3] Willert C E and Gharib M 1991 Digital particle image velocimetry *Exp. Fluids* **10** 181–93
[4] Adrian R J and Westerweel J 2010 *Particle Image Velocimetry* (Cambridge: Cambridge University Press)
[5] Raffel M, Willert C E, Scarano F, Kähler C J, Wereley S T and Kompenhans J 2018 *Particle Image Velocimetry: a Practical Guide* (Berlin: Springer)
[6] Keane R D and Adrian R J 1990 Optimization of particle image velocimeters. Part I: double pulsed systems *Meas. Sci. Tech.* **1** 1202–15
[7] Westerweel J 2008 On velocity gradients in PIV interrogation *Exp. Fluids* **44** 831–42
[8] Scharnowski S and Kähler C J 2016 Estimation and optimization of loss-of-pair uncertainties based on PIV correlation functions *Exp. Fluids* **57** 23
[9] Scharnowski S and Kähler C J 2016 On the loss-of-correlation due to PIV image noise *Exp. Fluids* **57** 119
[10] Scharnowski S, Grayson K, de Silva C M, Hutchins N, Marusic I and Kähler C J 2017 Generalization of the PIV loss-of-correlation formula introduced by Keane and Adrian *Exp. Fluids* **58** 150
[11] Grayson K, de Silva C M, Hutchins N and Marusic I 2018 Impact of mismatched and misaligned laser light sheet profiles on PIV performance *Exp. Fluids* **59** 2
[12] Nobach H and Bodenschatz E 2009 Limitations of accuracy in PIV due to individual variations of particle image intensities *Exp. Fluids* **47** 27–38
[13] Sciacchitano A, Wieneke B and Scarano F 2013 PIV uncertainty quantification by image matching *Meas. Sci. Tech.* **24** 045302
[14] Wieneke B 2015 PIV uncertainty quantification from correlation statistics *Meas. Sci. Tech.* **26** 074002
[15] Charonko J J and Vlachos P P 2013 Estimation of uncertainty bounds for individual particle image velocimetry measurements from cross-correlation peak ratio *Meas. Sci. Tech.* **24** 065301
[16] Xue Z, Charonko J J and Vlachos P P 2015 Particle image pattern mutual information and uncertainty estimation for particle image velocimetry *Meas. Sci. Tech.* **26** 074001
[17] Scharnowski S, Bross M and Kähler C J 2019 Accurate turbulence level estimations using PIV/PTV *Exp. Fluids* **60** 1
[18] Westerweel J and Scarano F 2005 Universal outlier detection for PIV data *Exp. Fluids* **39** 1096–100
[19] Adrian R J 1986 Image shifting technique to resolve directional ambiguity in double-pulsed velocimetry *Appl. Opt.* **25** 3855–8
[20] Scarano F 2001 Iterative image deformation methods in PIV *Meas. Sci. Tech.* **13** R1–19
[21] Masullo A and Theunissen R 2018 On dealing with multiple correlation peaks in PIV *Exp. Fluids* **59** 89
[22] Huang H, Dabiri D and Gharib M 1997 On errors of digital particle image velocimetry *Meas. Sci. Technol.* **8** 1427
[23] Christensen K T 2004 The influence of peak-locking errors on turbulence statistics computed from PIV ensembles *Exp. Fluids* **36** 484–97

[24] Michaelis D, Neal D R and Wieneke B 2016 Peak-locking reduction for particle image velocimetry *Meas. Sci. Technol.* **27** 104005

[25] Adrian R J 1997 Dynamic ranges of velocity and spatial resolution of particle image velocimetry *Meas. Sci. Tech.* **8** 1393

[26] Kähler C J, Scharnowski S and Cierpka C 2012 On the resolution limit of digital particle image velocimetry *Exp. Fluids* **52** 1629–39

[27] Westerweel J, Elsinga G E and Adrian R J 2013 Particle image velocimetry for complex and turbulent flows *Annu. Rev. Fluid Mech.* **45** 409–36

[28] Cuvier C *et al* 2017 Extensive characterisation of a high Reynolds number decelerating boundary layer using advanced optical metrology *J. Turbul.* **18** 929–72

[29] Sciacchitano A, Scarano F and Wieneke B 2012 Multi-frame pyramid correlation for time-resolved PIV *Exp. Fluids* **53** 1087–105